Sigma Journal of Engineering and Natural Sciences
Web page info: https://sigma.yildiz.edu.tr
DOI: 10.14744/sigma.2026.2071

Research Article

Estimating the performance of inter-connected square ring based flexible frequency selective surface which is insensıtıve to polarizatıon and oblique angles for EM shieldıng in wearable environment

P. VENKATESH[1,*]

[1]*Department of Electronics and Communication Engineering, Ramco Institute of Technology, Rajapalayam, 626117, India*

ARTICLE INFO

Article history
Received: 13 November 2025
Revised: 16 December 2025
Accepted: 17 January 2026

Keywords:
Angular Stability; Flexible; Frequency Selective Surface; Specific Absorption Rate (SAR); Wearable Electronics

ABSTRACT

Rapid development in high speed wearable electronics, on the other hand, puts health threats due to the radiation effects caused by the Antennas in the system. Hence, Electromagnetic (EM) radiation shielding continues to be an inevitable measure. To provide EM radiation shielding, the work proposed focuses on the design of Frequency Selective Surface (FSS) operating in a wide range of stopband. The fundamental method used for achieving wide stop band response is the square ring based method. Using the enhanced version of the square ring, wide stopband range from 3 to 18 GHz was achieved. The unit cell dimensions are 11x11 mm2, with a thickness of 0.8mm, developed in a completely flexible Jean material. To achieve wide stop band response, each stage in the design is connected with the previous stage. Due to the symmetric structure, the FSS remains insensitive to polarization. On minimizing grating lobes by maintaining proper periodicity, angular stability up to 80° has been achieved. A high shielding effectiveness of 40 dB has been achieved due to the minimum S21 values. Robust behavior is witnessed under bending scenario due to the flexible nature of the FSS. On-antenna verification is also carried out to verify the effectiveness of the FSS. 100% gain improvement and 70% efficiency improvement were witnessed. The average polarization shift and angle mean deviation were 4.2% and 3.8%, which were the most minimum values. The obtained simulation results were validated by an equivalent circuit model (ECM) and further confirmed through experimental results of the fabricated prototype. With these results achieved, the FSS remains as a promising candidate with wide stop band, high degree of angular stability with minimum polarization shift and angle mean deviation.

Cite this article as: Venkatesh P. Estimating the performance of inter-connected square ring based flexible frequency selective surface which is insensıtıve to polarizatıon and oblique angles for EM shieldıng in wearable environment. Sigma J Eng Nat Sci 2026;44(3):1903−1914.

INTRODUCTION

Due to the rapid advancement in wireless technologies and the associated need for improved healthcare units, wearable electronics with communication capabilities has gained a lot of attention. Wearable communication has paved way to overcome the conventional methods of

***Corresponding author.**
*E-mail address: venkateshp286@gmail.com

This paper was recommended for publication in revised form by Editor-in-Chief Ahmet Selim Dalkilic

Published by Yıldız Technical University Press, İstanbul, Turkey
© Author. This is an open access article under the CC BY-NC license (http://creativecommons.org/licenses/by-nc/4.0/).

human monitoring which makes the health sectors over crowded [1]. A sample image in Figure 1 shows the devices accompanied for wearable communication.

It can be clearly invoked from the figure that, a wearable system eventually requires an appropriate antenna to transmit and receive human physiological data. But the issue in the antennas deployed in wearable systems is its undesired radiation effects, that it exerts towards the human body. Hence, a suitable shielding methodology is required to shield the human body from superfluous radiation effects [2]. For wearable applications, the shield used should also be flexible, light weight, compact, insensitive to polarization and oblique angle incidence [3], as well. In antenna's perspective, Electromagnetic shielding shall be carried out using simple dielectric shielding [4,5] metasurface [6], Artificial Magnetic Conductors [7]. But the above mentioned methods require complex vias, ground planes and three-layer design. Also they don't focus on angular stability and polarization insensitivity. Hence, the idea of FSS has become dominant due to its versatile design opportunities which are not available with the above mentioned techniques.

According the fundamental definition, FSS are 2D periodic structures arranged in a particular manner over a dielectric surface without any ground plane. They exhibit both transmission and reflection behavior depending on the design made, wherein the patch type FSS exhibit reflection behavior while the slot type FSS exhibit transmission behavior [8]. As most of the wearable applications work in ISM band, the intended FSS were designed to operate only in a very narrow band as in [9,10]. But, due to the rapid development of wideband and high speed systems, research focus turned to come up with wideband FSS design. Most commonly, Wideband FSS were designed using stacked layers of dielectric as in [11,12] or multilayer FSS model as in [13,14,15]. But, development of such FSS models leads to low profile issues, which is one of the main counterparts in wearable applications.

Later on, convoluted FSS structures were deployed to achieve wide band stop response. A convoluted FSS design with dual layers of patches was proposed in [16]. The design covered the dual band, yet with the limitations of wideband. FSS with simple convoluted square structure and central slots was proposed in [17], which covered the upper limit of UWB spectrum. Nevertheless, the design complexity was increased in both the aforementioned works, which is a notable shortfall.

The FSS design proposed in [18] is quite simple, where the nearby adjacent square rings are interconnected with each other for improving the stop bandwidth. Because of the demand in interconnection, more square rings are required, which in turn increases the overall area. The FSS proposed in [18] is developed with a modified square loop, where, the half the portion of the patch was engraved along every arm of the FSS [19]. However, the FSS shall not be a suitable candidate for wearable shielding applications because of the rigid nature of the substrate. In [20], ultra wide band stop response was achieved using two cascaded layers. Also the polarization sensitivity was not estimated in the work. By printing orthogonal FSS array along the same side of the substrate, wide band stop response was achieved in [21] with some sacrifice in size constraints. In [22], edges of square ring were connected with other parts

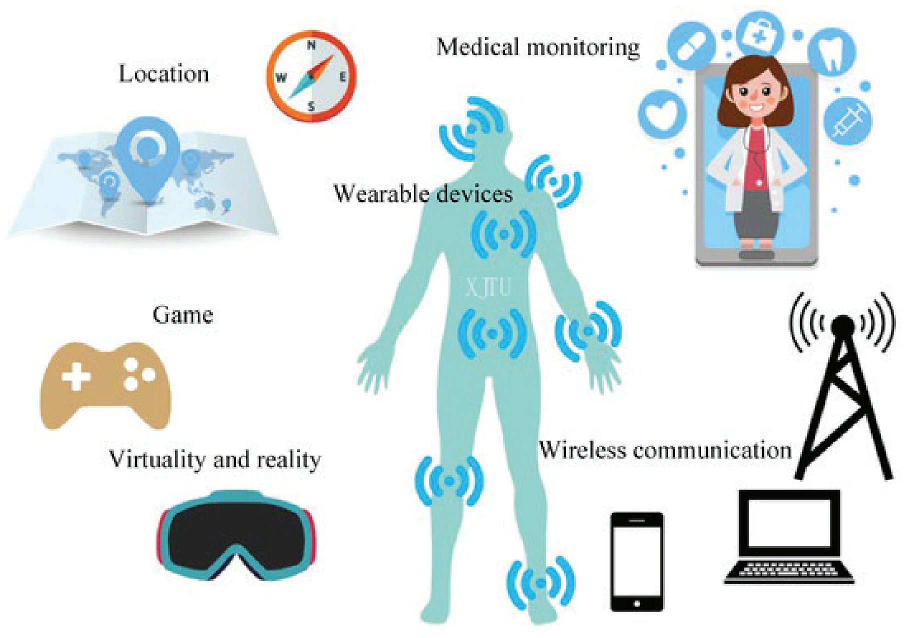

Figure 1. A sample wearable communication scenario.

of the patches to achieve wide stop band up to 13 GHz. But, the FSS is not completely flexible.

All the FSS reported above lack complete flexible nature on its behalf. Also, the stacking layers of substrate and encompassing dual metallic layers, eventually raises size constraints. Limitations in polarization insensitivity, angular stability, shielding effectiveness, robust bending performance exists as well.

Hence, getting motivated in overcoming the shortfalls with the works reported in the literature, a completely flexible FSS with wide band stop response, appreciable polarization insensitivity and angular stability in both flat and bending scenarios, good shielding effectiveness, minimum polarization shift and angle mean deviation, is proposed in this work. The application of proposed FSS design, in this paper, is to provide shielding of Electromagnetic waves in wearable systems. This shielding reduces the radiation related health hazards with minimum SAR. FSS can also be applied to improve the antenna performance, which is also discussed in this manuscript. Apart from the aforementioned applications, FSS finds its application in wide aspects like aircraft radome for protection, RADAR cross section reduction, Frequency selective walls and windows, absorbers, rasorbers and polarization manipulation [8]. The script is structured with the FSS design part in section 2, free space and Antenna-FSS performance in sections 3 and 4 respectively.

MATERIALS AND METHODS

FSS are 2D periodic structures used to provide EM radiation shielding and enhance the antenna performance in diverse aspects. The objective of deploying FSS with antenna is to restrain the SAR by reflecting the EM waves moving towards the human body. This also helps in supporting off body communication [22].

Unlike the usage of stacked layers [11,12] or multi layered FSS as in [13-15] for wideband response, a novel approach of inter-rotated squar ring with corner connected stubs was executed. The proposed FSS structure is depicted in Figure 2 [23]. The structure of FSS was inspired and initiated with a simple square ring model as it is suggestive for wideband operation [24]. The simulation environment of the proposed FSS was executed using Computer Simulation Technology (CST) with completely flexible textile Jean material whose dielectric constant is 1.67. This is shown in Figure 3. Two ports namely Zmax and Zmin were setup at the front and rear sides of the structure which acts as input and output port respectively. The FSS structure is placed at a distance of λ/4 from the input port.

The design evolutionary stages of the FSS and its transmission characteristics (S_{21}) are displayed respectively in figure 4 and 5. The electrical length of the square ring shall be estimated using equation 1.

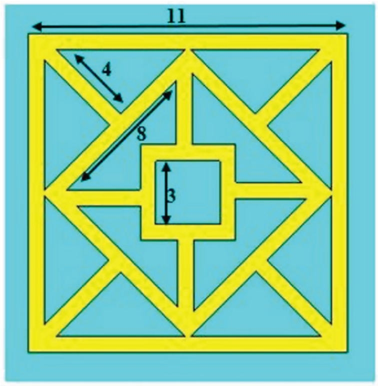

Figure 2. Proposed FSS structure.

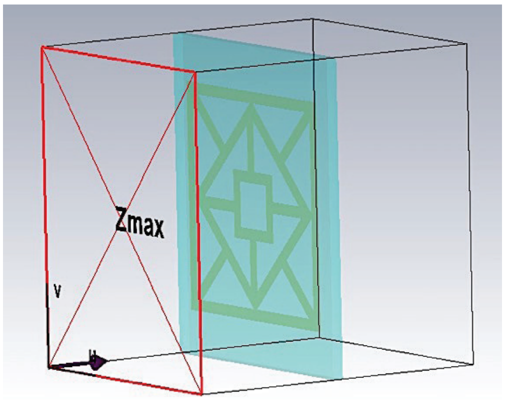

Figure 3. FSS simulation setup.

$$f_r = \frac{C}{4L\sqrt{\frac{\varepsilon_{eff}+1}{2}}} \quad (1)$$

By choosing the periodicity ‘p’ of the FSS structure as in the inequality [24], grating lobes are minimized

$$p(1+\sin\theta) < \lambda_0 \quad (2)$$

Where λ_0 is the wavelength of freespace. On satisfying the above inequality, the periodocity is estimated as [24]

$$p = M\lambda_0 \quad (3)$$

Using this deception, the FSS ring width is estimated using the equation in (4)

$$1 = 4\left(\frac{L}{\lambda_0}\right)^2 \ln\left(\frac{2M\lambda_0}{\pi w}\right) \quad (4)$$

Where ‘w’ is the width of FSS ring and ‘M’ is an arbitrary constant between 0 and 1 [24].

To begin the design, the frequency of operation is taken to be 5 GHz. With a string resonance around 5 GHz, a stop

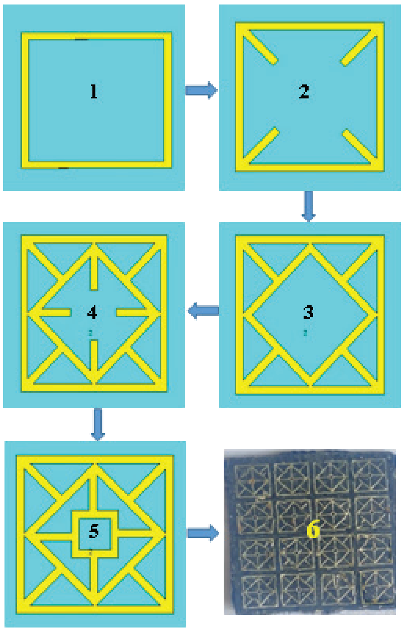

Figure 4. Design stages of FSS.

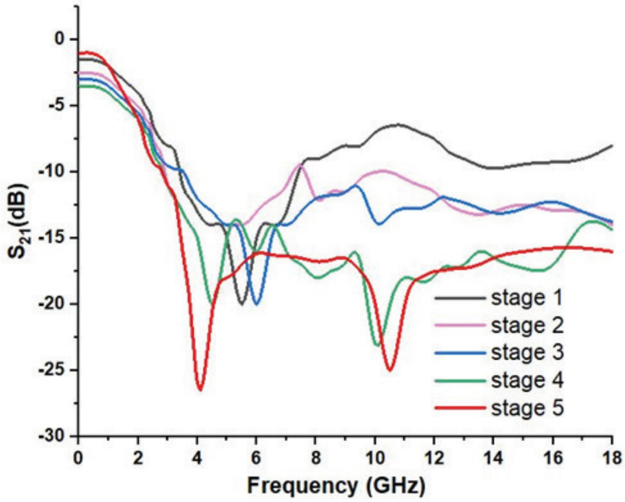

Figure 5. S_{21} of FSS design.

band from 3.49 to 7 GHz was obtained in stage 1 of the design [25]. Keeping in mind two facts, namely, reduction

of spurious corner radiation and bandwidth enhancement, 4 stubs were extended from the corners of the square ring [26], in stage 2. Because of this, the lower end frequency shifted to 2.9 GHz while the upper end shifted to 6.8 GHz. In stage 3, for resonance enhancement at high frequencies, another square was joined with the stubs in stage 2, with 45° rotation. This inproves the length of the current path, and so, the upper end frequency extended to 12.9 GHz, but the lower end also shifted to 3.5 GHz. To again take the lower frequency band to further lower side, the same approach of using 4 stubs from the corner was deployed in fourth stage, which shifted the lower end to 3.05 GHz. To further enhance the bandwidth and maintain the symmetry of the structure, another small square ring was fused with the 4 stub corner. As a result, the electrical path taken by the current was significantly improved, and because of this current path extension, with comparitielvy smaller square length, the upper frequency range was extended to 18.15 GHz, while the lower frequency edge was almost the same [24]. Now, with the final design, the proposed FSS was able to provide ultra wide stop band response from 3.1 to 18.15 GHz. Stage 6 in the Figure 4 shows the fabricated prototype of FSS.

The gap 'g' behind between each FSS unit cell in the FSS array, was set to be greater than the ringth width 'w', so that, the ratio $2p/\pi w$ shall be dominatin over the ratio $2p/\pi g$. This condition is to ensure minimum grating lobes, which is an important factor for robust FSS performance [25].

Now, with the prediction in equation (4), a careful parametric analysis is done to ascertain the reliable values for w, as it plays a major role in impedance matching (Fig. 5). The analysis was carried out with three width values 0.25, 0.35 and 0.5 mm. The result of the parametric analysis is depicted in Figure 6. With reference to -15 dB isolation limit, width of 0.25 mm results in poor impedance matching around 4 to 7 GHz. It is also noted that, for the widths 0.35 and 0.5 mm, the results are almost same. Hence, keeping in mind the size constraints, the optimum value of 0.35mm has been chosen.

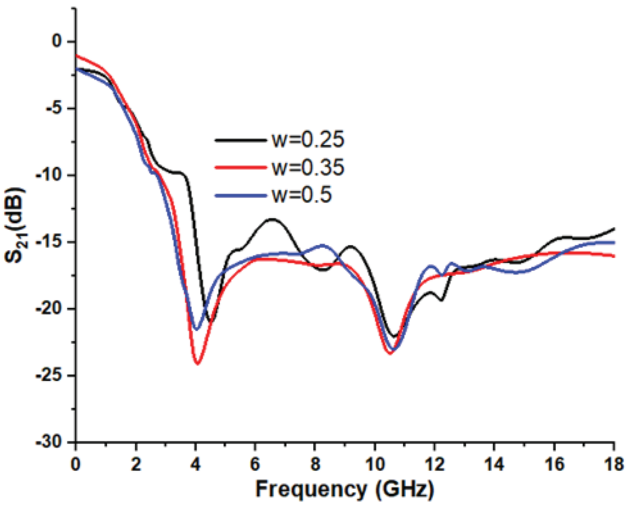

Figure 6. Parametric analysis of width 'w'.

RESULTS AND DISCUSSION

The proposed FSS is fabricated using the Jean substrate with 4x4 elements with an overall layout of 50 x 50 mm2. As the FSS in this manuscript is aimed for antenna based applications, choosing 4x4 periodicity shall be better choice, keeping in in mind the space constraints and average antenna geometry. Before moving to fabrication, the equivalent circuit of the proposed design was estimated and analysed using cadence virtuoso environment.

Reflection Behavior

The equivalent circuit has been approximated by starting with the outer most part of the FSS. The outer most larger square and the four corner stubs in stage 2 are modelled as two inductors in series and the gap between them is modelled as a capacitor. Similarly, the rotated square and the 4 corresponding stubs associated with it, as seen in stage 4, are modelled as two inductors and one capacitor. Finally, in stage 5, since one small square ring alone is modelled without any stubs being connected to it, it is modelled as one inductor and a capacitor. With this idea, the overall circuit is shown in Figure 7.

The RLC equivalent model of the proposed FSS is simulated for its resonance characteristics using cadence virtuoso environment. For measurements, the proposed FSS is placed between two horn antennas. The transmitted and reflected waves are collected from the N9951A network analyzer connected to the measurement setup.

The sample block diagram for carrying out measurement and the actual measurement in anechoic chamber is shown in Figure 8. The comparison between the EM simulation results from CST and RLC model results are depicted in Figure 9 along with the measured results. The results show that the measurement data is well agreeing with the simulated data, with minimum variations arose due to dielectric loss. This proves the applicability of FSS in realtime environment.

Polarization Insensitivity

In certain scenarios like body centric applications, the FSS orientation and the fixed position of the FSS shall tend to change, because of the rapid & random movement of the human body, which would affect the FSS response. To verify this, polarization insensitivity and FSS response for various incidence angles are studied.

Figure 10 shows the stop band of the FSS for both TE polarization and TM polarization. The S_{21} response preferably overlaps each other thereby confirming the robust

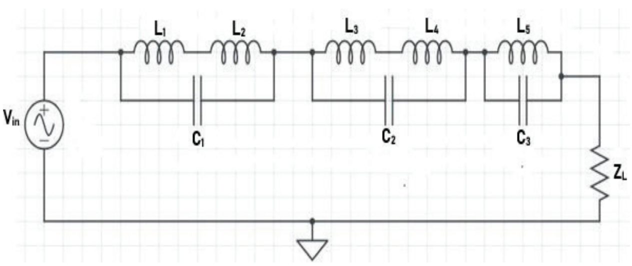

Figure 7. Equivalent circuit model of FSS.

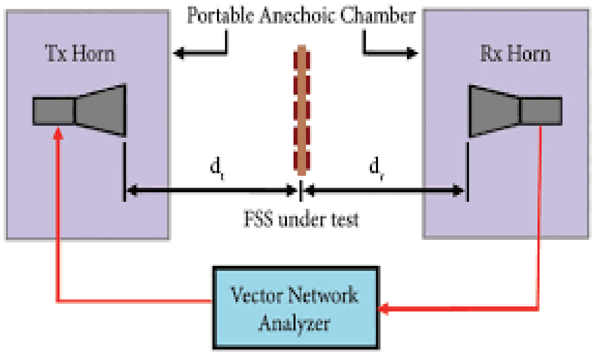

(a)

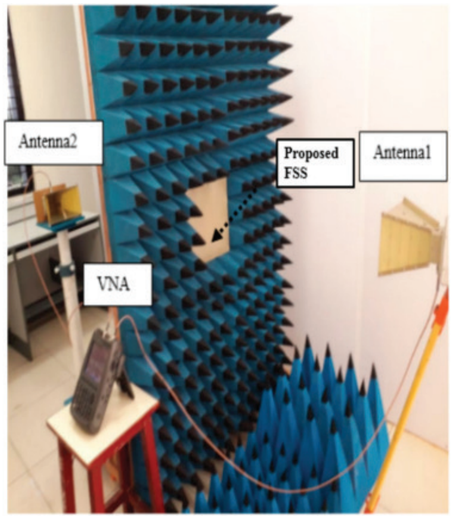

(b)

Figure 8. Measurement of FSS (a) Block diagram (b) actual measurement.

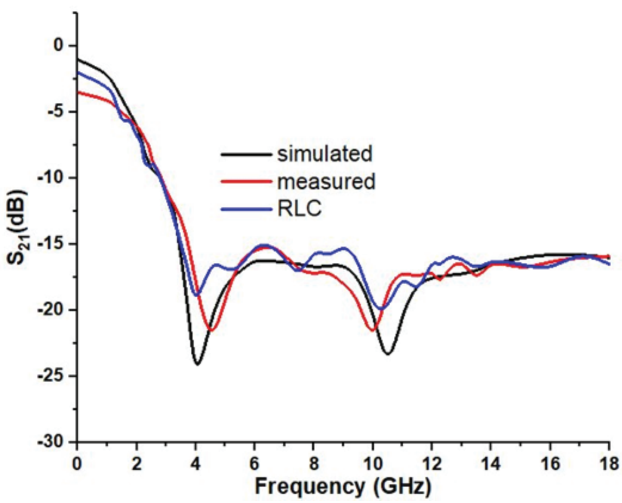

Figure 9. S_{21} of the proposed FSS.

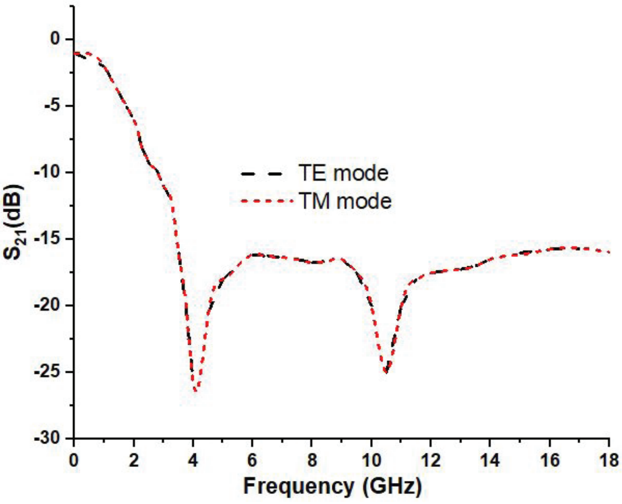

Figure 10. S_{21} response for TE and TM modes.

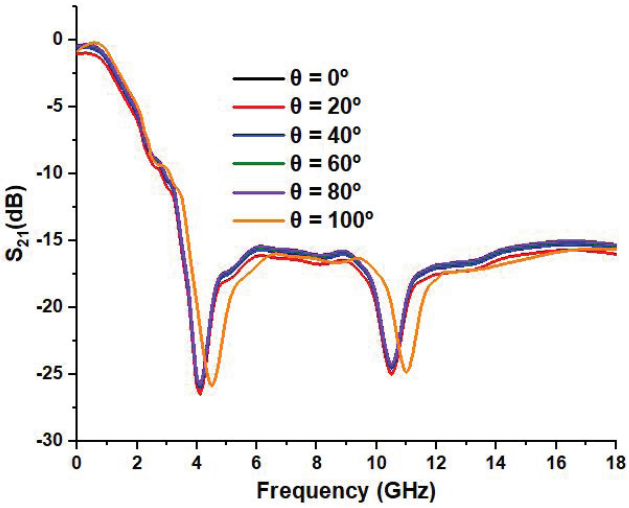

Figure 12. FSS response for varying incident angles under TM mode.

stop band in both TE and TM polarization modes. Hence, the proposed FSS design is insensitive to any kind of polarization [25].

Angular Insensitivity

Also, the response of the proposed FSS was verified with different incident angles of the impinging signal. This is because, the incident EM wave on the FSS shall be at any tilted angle depending up on the configuration of the source from where it arises. But the response of the FSS structures should not deviate much in such cases. The simulated response of the proposed FSS for various angles of incidence under TE and TM polarization modes are respectively depicted in Figures 11 and 12.

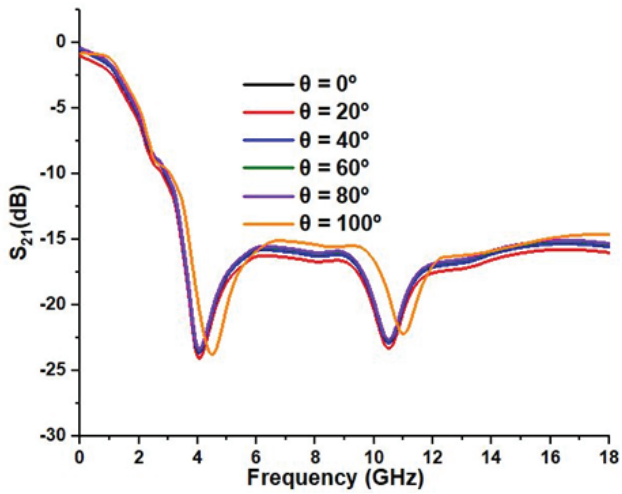

Figure 11. FSS response for varying incident angles under TE mode.

On looking at response, it apparent that the proposed FSS design exhibits stable reflection behavior upto an angle of 80°. This is due to the summetric nature of the design, thanks to it. A slight deviation occurs only for the angle 100°, which could be due to the varying current nature at the edges at high frequencies.

This shows that the FSS is maximally tolerant to an oblique angle incidence of up to 60°, with slight acceptable variations till 80°. The better polarization stability and high degree of angular stability is because of the symmetric nature of the FSS design structure (providing same view from all directions).

Shielding Effectiveness

The FSS ability to shield the electromagnetic signal is given in terms of Shielding Effectiveness (SE), which is calculated using the equation in 14.

$$SE\ (dB) = -20 \log \left[\frac{E_t}{E_i}\right] \tag{5}$$

Where, Et stands for transmitted wave from the FSS and Ei is the incident wave impinging on the FSS. The SE this obtained is represented in Figure 13. From Figure 13, it is clear that the proposed FSS exhibits appreciable SE, above 40 dB [26], in its operating range. This high shielding effectiveness is because of the minimum S21 values, as seen from Figure 13.

Bending Performance

As the proposed FSS is intended for wearable applications, it becomes inevitable to analyze the characteristics of FSS under some bent conditions. This is because, the surface of the human body, where the wearable component will be placed, is not flat thought. The bending is performed in two orientations namely x-bend and y-bend. The sample

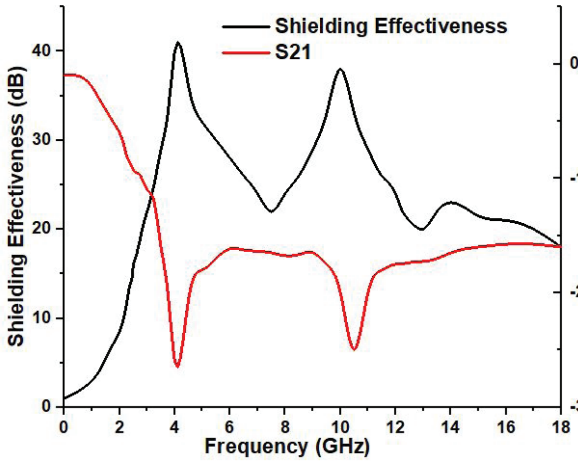

Figure 13. Shielding Effectiveness of FSS.

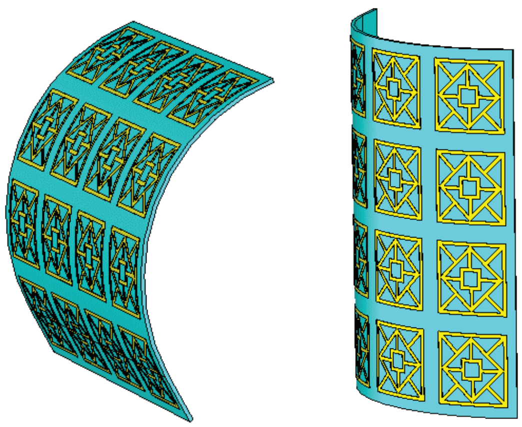

(a) (b)

Figure 14. FSS bending (a) X-bend (b) Y-bend.

images in bending the FSS is shown in Figure 14. Three bending dimensions namely, 50mm, 75mm and 125mm, were chosen based on the approximate dimensions of arm, thigh and wrist of an adult, as in Figure 14.

The results clearly indicate that the reflective nature of the FSS withstands well. For 50mm bending, no notable variations exist in both x and y bend. Only minimum frequency shifts are experienced for 75mm bending. In x bend, a slight shift from 3.1 to 3.25 GHz in noticed and in y bend, the same shift is seen along with a slight shift at high frequencies. But for 125mm bending, reasonable shift happens around 3 to 4 GHz in x bend and at high frequencies poor impedance match is seen after 14 GHz. For y bend, with the same radius, frequency shift occurs from 3 to 4.2 GHz and poor matching is seen after 15 GHz too. of arm, thigh and wrist of an adult, as in Figure 14. The obtained reflection characteristics (S_{21}) under bent condition and its

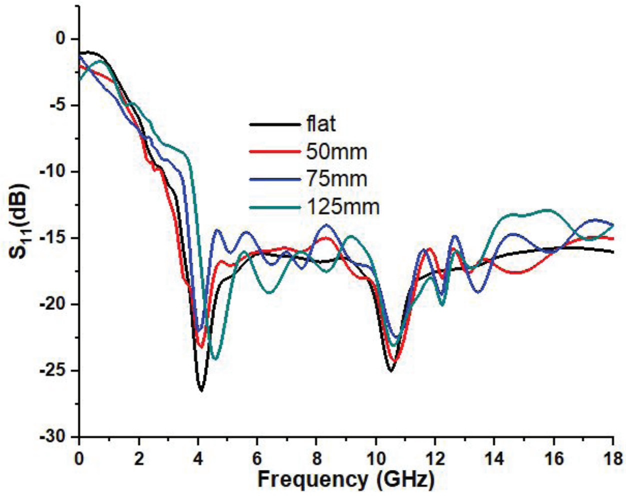

Figure 15. S_{21} for x bend.

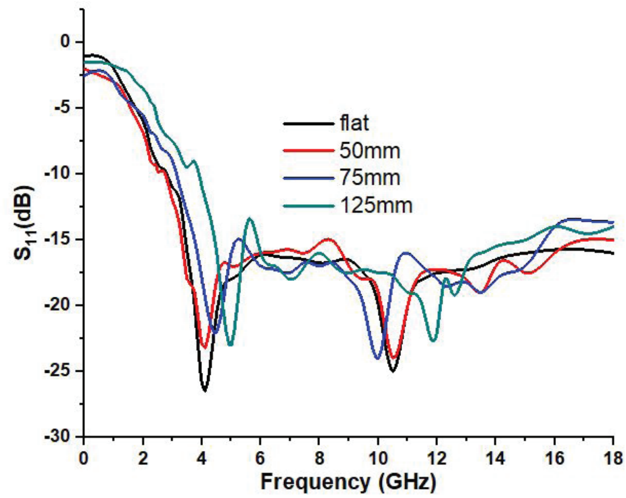

Figure 16. S_{21} for y bend.

comparison with the flat result is depicted in Figure 15 and 16 for x bend and y bend respectively.

The reason for shift is the sensitivity of current along the edges of the unit cell. Changes in effective length along the edges causes a shift in resonance leading to degradation in overall bandwidth [7]. But, the reduced bandwidth still covers the entire UWB spectrum, except for 125mm bending.

To estimate how much shift has occurred in FSS polarization, the average polarization shift is used. Numerically, the average shift in polarization is estimated using equation 6.

$$\Delta f_{\theta} = \frac{\Sigma_{1}^{N}\frac{f_{\theta}^{TM} - f_{\theta}^{TE}}{f_{\theta}^{TM}}}{N} X\,100 \quad (6)$$

Where, f_{θ}^{TM} and f_{θ}^{TE} are the centre frequency of TE and TM for various θ values and N is the average oblique incident angles considered. Using equation 15, the estimated shift was found to be 4.2%, which is quite low and appreciable.

The angle mean deviation represents the deviation of FSS response under various oblique incident angles from the frequency response under normal incidence. It is estimated using the relation given in equation 7.

$$\%\delta f_p = \frac{\sum_{i=1}^{N} f_p^{normal} - f_p^{ai}}{N * f_p^{normal}} X100 \quad (7)$$

Where, p is the mode (TE/TM), f_p^{normal} is the frequency response of FSS under normal incident angle and f_p^{ai} is the frequency response at various oblique angles. The computed percentage deviations are 3.85 and 4.15 % respectively for TE and TM modes. Such a minimum deviation confirms the suitability of the proposed FSS for EM shielding under various oblique cases.

On Antenna Performance

In order to verify the performance of the FSS on the vicinity of antennas, the proposed FSS is placed behind a sample antenna and certain results like S_{11}, gain, efficiency and SAR were analyzed. This antenna-FSS configuration is shown in Figure 17. The antenna with its dimensions and the fabricated antenna are shown in Figure 18 and 19 respectively. The antenna is fed by a 50Ω microstrip feed line. The substrate used for the design is flexible textile Jean material whose dielectric constant is 1.67. The antenna is a circular patch antenna with slots in the patch to enhance the bandwidth at high frequencies. Partial and stubbed ground plane are deployed for improving impedance matching at low frequencies. The simulated and measured return loss of the antenna is depicted in Figure 20. The antenna extends its operating wideband resonance from 3 GHz to

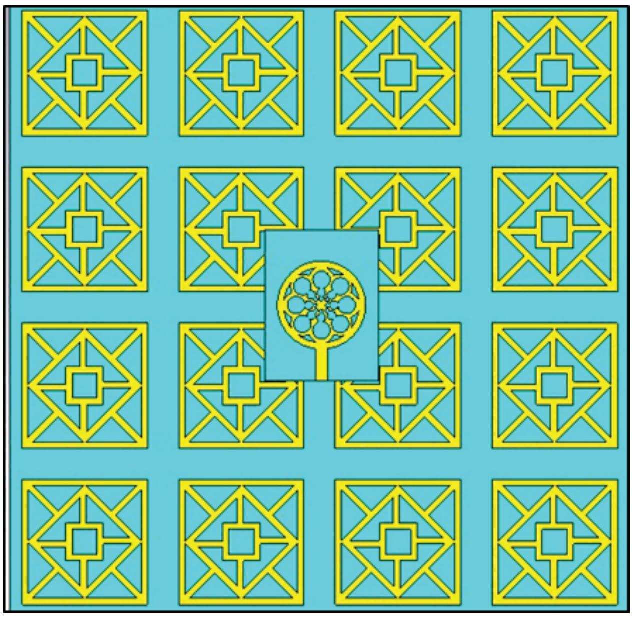

Figure 17. Antenna-FSS set up.

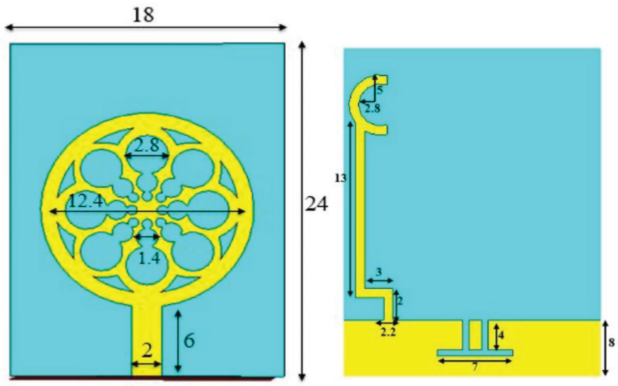

Figure 18. Antenna-dimensions.

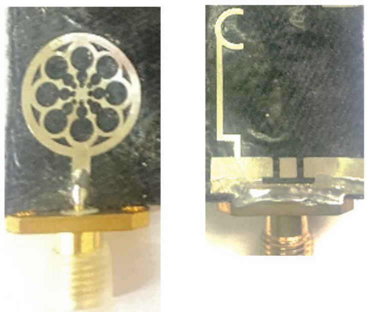

Figure 19. Fabricated antenna

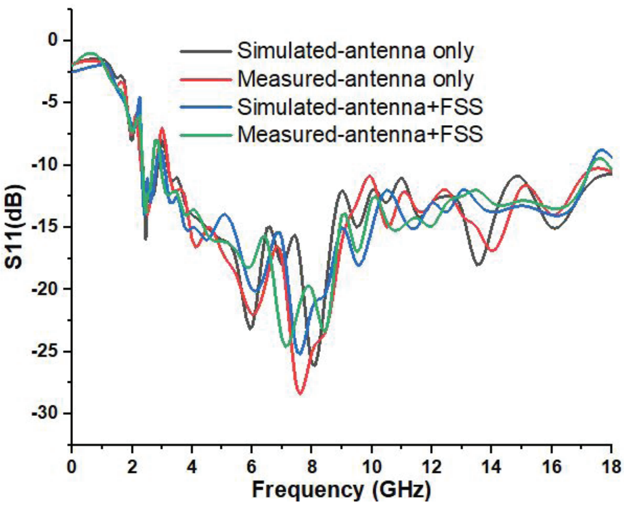

Figure 20. Antenna return loss.

17.75 GHz. From the results it is clear that the antenna does not exhibit much deviation when integrated with the FSS, which is a notable advantage. This is because, λ/2 distance (15mm) is properly maintained between the antenna and FSS [11] . The radiation pattern of the antenna is depicted in Figure 21. The pattern is bi-directional and the pattern was reformed to unidirectional by using the FSS behind the antenna. This shows that the FSS significantly reduces the back radiation from the antenna.

With this, the antenna was simulated and measured to verify the positive impact of FSS with respect to its gain, efficiency and Specific Absorption Rate (SAR). The gain and efficiency are depicted in Figure 22 and 23 respectively, while the SAR values are tabulated in Table 1.

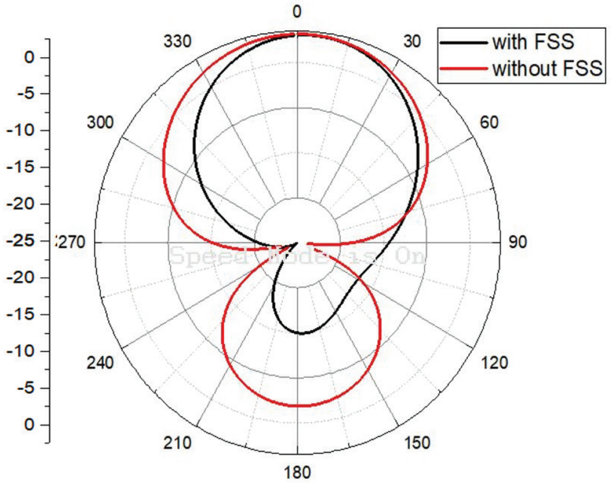

Figure 21. Antenna radiation pattern.

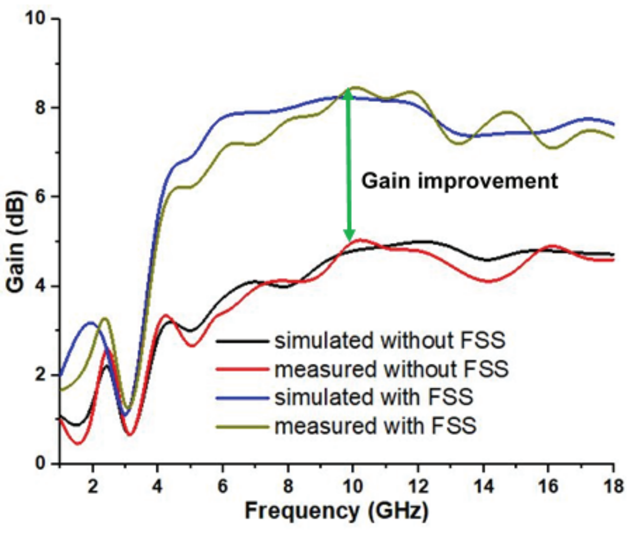

Figure 22. Antenna – FSS gain improvement.

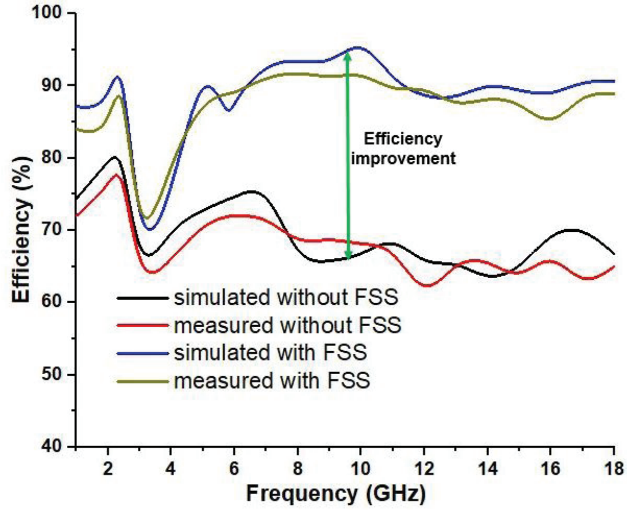

Figure 23. Antenna – FSS efficiency improvement.

Table 1. SAR effects

Frequency (GHz)	SAR (W/Kg)			
	Without FSS		With FSS	
	2mm gap	5mm gap	2mm gap	5mm gap
2.45	1.82	1.55	1.214	0.698
5.8	2.75	2.03	0.827	0.326

It is obvious to note that the peak gain of the antenna which was 4.5 dB without deploying FSS has now improved to 9.1 dB on placing the proposed FSS behindhand. It has been proved that the proposed FSS resulted in 100% gain improvement henceforth. Likewise, the efficiency of the antenna, which was 66%, was then elevated to 95% with the advent of FSS. This confirms the strong reflective nature of the proposed FSS with constructive interference. To further verify the FSS performance, the same antenna was simulated for SAR estimation, under with and without FSS conditions. For SAR estimation, the methods and tissue model suggested in [27,28] was followed. As tabulated in 1, it is clear that, for varying gaps between antenna and FSS, the SAR values are substantially reduced. This proves that the proposed FSS is a highly suitable candidate for EM radiation shielding in wearable applications.

A comparative analysis of the proposed FSS metrics, with the other existing FSS in the literature is presented in Table 2. Based on this comparison with the existing works, it could be invoked that the proposed FSS is smaller in dimensions with single layer and reduced thickness, along with wide band stop response and conformal nature. In the thickness aspect, the proposed design remains with most lower thickness which is required for wearable systems. On comparing the FSS dimensions, the proposed work remains

Table 2. Performance comparison

Reference	Thickness (mm)	FSS dimensions (mm²)	Structures deployed	Number of layers	*NB or WB/ Max. Stop Bandwidth (GHz)	Flexible	Polarization insensitivity	Angular stability	On-Antenna test
[3]	2.10	18x18	Extended cross dipole	2	NB/0.4	Yes	Yes	60°	No
[10]	1.6	38.5x38.5	Star shaped	1	WB/6	Yes	Yes	45°	No
[11]	1	11x11	Square ring	2	WB/12.25	No	*NE	NE	No
[16]	1	10x10	Convoluted structure	1	NB/0.75	No	Yes	45°	No
[17]	1.6	8x8	Side connected square ring	1	WB/14	No	Yes	80°	No
[20]	1.6	10x10	rectangular loop pair	1	WB/9	No	No	No	No
[23]	*NS	12.57x12.57	Swastika shape	1	NB/1.6	No	Yes	45°	No
Proposed	**0.8**	**11x11**	**Modified square ring with stubs, 4x4 FSS**	**Single**	**15**	**Yes**	**Yes**	**80°**	**Yes**

better than the existing works except [16] and [17]. But [16] and [17] don't provide flexibility, which the proposed work does. The proposed FSS provides more operating bandwidth and better angular stability, compared to all the existing works listed. No existing work reported in the literature has performed on-antenna verification, while, in this work, on-antenna test has been carried out. This is a notable superiority and novelty of the proposed work.

CONCLUSION

This article discussed about a compact, flexible Frequency Selective Surface (FSS) for EM shielding in entire UWB band. The design was developed for wide band stop response, achieved by connecting each square ring with other via stubs. With this design, the transmission coefficient characteristics was extended from 3 GHz to 13 GHz. The same was verified with ECM and fabricated model, where the obtained results were close enough to the simulated ones. Irrespective of the polarization considered, 80° angular stability was achieved by the proposed FSS. The same response was found to be robust under bending radius of up to 100mm. The numerically computed average polarization shift and angle mean deviation were found to be 4.2 and 3.85% respectively, which are substantially low. The on-antenna performance of the FSS also proved that deputing FSS beneath the antenna vicinity resulted in 100% improvement in gain, 95% improvement in efficiency with a maximum of 83% SAR reduction. Based on the ability of the FSS to retain the required band stop behaviour, it shall be a pretty good candidate for EM shielding under entire UWB spectrum.

Despite of the ultra-wide stop band response, polarization insensitivity, enhanced angular stability, satisfactory shielding effectiveness, yet, certain directions remain open for future research. The proposed design, being passive, can be extended as active FSS by integrating PIN diodes, MEMS devices which allows to integrate reconfigurable features with the proposed FSS. Beam steering of the reflected wave from FSS is also possible by this active FSS configuration. Furthermore, the periodicity of FSS shall be improved further to enhance the shielding effectiveness, gain and efficiency. Also, by making the FSS a dual layer FSS, simultaneous transmission and reflection control can be achieved, with a considerable sacrifice in overall thickness of the structure.

DATA AVAILABILITY STATEMENT

The authors confirm that the data that supports the findings of this study are available within the article. Raw data that support the finding of this study are available from the corresponding author, upon reasonable request.

CONFLICT OF INTEREST

The author declared no potential conflicts of interest with respect to the research, authorship, and/or publication of this article.

ETHICS

There are no ethical issues with the publication of this manuscript.

STATEMENT ON THE USE OF ARTIFICIAL INTELLIGENCE

Artificial intelligence was not used in the preparation of the article.

REFERENCES

[1] Yadav A, Kumar Singh V, Kumar Bhoi A, Marques G, Garcia-Zapirain B, de la Torre Díez I. Wireless body area networks: UWB wearable textile antenna for telemedicine and mobile health systems. Micromachines 2020;11:558. [CrossRef]

[2] Chauraya A, Seager R, Whittow W, Zhang S, Vardaxoglou Y. Embroidered frequency selective surfaces on textiles for wearable applications. LAPC 2013 - 2013 Loughborough Antennas and Propagation Conference 2013;388–391. [CrossRef]

[3] Viswanathan L, Kanagasabai M, Mohammed GNA. Conformal ultra-miniaturized frequency selective surface for medical shielding applications. International Journal of Communication Systems 2024;37:e5790. [CrossRef]

[4] Veeraselvam A, Mohammed GNA, Savarimuthu K, Marimuthu M, Balasubramanian B. Polarization diversity enabled flexible directional UWB monopole antenna for WBAN communications. International Journal of RF and Microwave Computer-Aided Engineering 2020;30:e22311. [CrossRef]

[5] Venkatesh P, Narmadha T. Design of a compact sigma slotted dual-mode UWB antenna for wireless body area network applications. International Journal of Microwave and Wireless Technologies 2023;1–14. [CrossRef]

[6] Pandi Ravichandran V, Velayudham N, Velayudham P. On the design and analysis of a miniaturized ultra-wideband (UWB) antenna using quatrefoil-shaped nonuniform meta-surfaces for body-centric communications. International Journal of Communication Systems 2024;37:e5712. [CrossRef]

[7] Pandi Ravichandran V, Velayudham N. On the performance investigation of a low profile UWB antenna backed with conjointly connected sickle shaped AMC structure for on-/off body communications. Frequenz 2025;79:353–372. [CrossRef]

[8] Munk BA. Frequency selective surfaces: Theory and design. New York: Wiley; 2005.

[9] Sugumaran B, Balasubramanian R, Palaniswamy SK. Performance evaluation of compact FSS-integrated flexible monopole antenna for body area communication applications. International Journal of Communication Systems 2022;35:e5085. [CrossRef]

[10] Renit C, Raj TAB. Wearable frequency selective surface-based compact dual-band antenna for 5G and Wi-Fi applications. Automatika 2024;65:454–462. [CrossRef]

[11] Bhattacharya A, Dasgupta B, Jyoti R. A simple frequency selective surface structure for performance improvement of ultra-wideband antenna in frequency and time domains. International Journal of RF and Microwave Computer-Aided Engineering 2021;31:e22857. [CrossRef]

[12] Montejo-Garai JR, Page JE, Perez-Palomino G, Guirado R. Band-stop frequency-selective surface (FSS) with elliptic response designed by the extracted pole technique. Sensors 2024;24:4452. [CrossRef]

[13] Kushwaha N, Kumar R, Oli T. Design of a high-gain ultra-wideband slot antenna using frequency selective surface. Microwave and Optical Technology Letters 2014;56:1498–1502. [CrossRef]

[14] Ranga Y, Matekovits L, Weily AR, Esselle KP. A low-profile dual-layer ultra-wideband frequency selective surface reflector. Microwave and Optical Technology Letters 2013;55:1223–1227. [CrossRef]

[15] Kışla BC, Şenel B. Double-sided bandpass frequency selective surface design for C band WLAN radome applications. Sigma Journal of Engineering and Natural Sciences 2025;43:2263–2271. [CrossRef]

[16] Habib S, Kiani GI, Butt MFU. A convoluted frequency selective surface for wideband communication applications. IEEE Access 2019;7:65075–65082. [CrossRef]

[17] Jeyaraman D, Santhanam S. Equivalent circuit model for convoluted meander line frequency selective surface for multi-frequency applications. ACES Journal 2024;39:581–592. [CrossRef]

[18] Paul GS, Mandal K, Lalbakhsh A. Single-layer ultra-wide stop-band frequency selective surface using interconnected square rings. AEU - International Journal of Electronics and Communications 2021;132:153630. [CrossRef]

[19] Katoch K, Jaglan N, Gupta SD. Design and analysis of single sided modified square loop UWB frequency selective surface. IEEE Transactions on Electromagnetic Compatibility 2021;63:1423–1422. [CrossRef]

[20] Sarika, Tripathy MR, Ronnow D. A wideband frequency selective surface reflector for 4G/X-band/Ku-band. Progress in Electromagnetics Research C 2018;81:151–159. [CrossRef]

[21] Verma AK, Singhal R. Performance analysis of frequency selective reflectors based on rectangular loop pair for wideband applications. AEU - International Journal of Electronics and Communications 2023;167:154675. [CrossRef]

[22] Mondal K. Polarization-insensitive large-scanning-angle broadband-stop frequency-selective surface for electromagnetic shielding. Journal of Computational Electronics 2024;23:153–159. [CrossRef]

[23] Venkatesh P, Narmadha TV, Ponnrajakumari M, Loganathan K. Time domain and qualitative analysis of a compact asymmetrically fed circular UWB antenna for WBAN scenarios. International Journal of Electrical and Computer Engineering Systems 2025;16:39–51. [CrossRef]

[24] Jha KR, Singh G, Jyoti R. A simple synthesis technique of single-square-loop frequency selective surface. Progress in Electromagnetics Research B 2012;45:165–185. [CrossRef]

[25] Venkatesh P, Ponnrajakumari M, Narmadha TV, Ramasamy R, Radhika SA, Padmavathy TV. On attempting to improve the reliability in body-centric communications using fully flexible diversified quad-port MIMO antenna backed with FSS. International Journal of Microwave and Wireless Technologies 2025;1–23. [CrossRef]

[26] Venkatesh P, Narmadha TV. Miniaturized trib-and planar monopole antenna using right turned L-shaped stubs for wireless communications. 2022 Fourth International Conference on Emerging Research in Electronics, Computer Science and Technology (ICERECT) 2022;1–6. [CrossRef]

[27] Venkatesh P, Narmadha TV. Performance analysis of a low profile UWB antenna with equivalent circuit based EBG modelling for WBAN communications. Sādhanā 2025;50:232. [CrossRef]

[28] Padmavathy TV, Venkatesh P, Bhargava D, et al. Design of I-shaped dual C-slotted rectangular microstrip patch antenna (I-DCSRMPA) for breast cancer tumor detection. Cluster Computing 2019;22:13985–13993. [CrossRef]

[29] Sağ RN, Tüylü T, Çalışkan A, Türker Tokan N. High gain, low-profile, wideband Archimedean spiral antenna with hexagonal fractal reflector surface. Sigma Journal of Engineering and Natural Sciences 2025;43:878–886. [CrossRef]